Dyes and Pigments 94 (2012) 239–246

Contents lists available at SciVerse ScienceDirect

Dyes and Pigments

journal homepage: www.elsevier.com/locate/dyepig

Cu^{2+} fluorescent sensor based on mesoporous silica nanosphere

Deli Lu, Juying Lei, Zhidan Tian, Lingzhi Wang*, Jinlong Zhang*

Key Lab for Advanced Materials and Institute of Fine Chemicals, East China University of Science and Technology, 130 Meilong Road, Shanghai 200237, PR China

ARTICLE INFO

Article history:
Received 8 November 2011
Received in revised form
6 January 2012
Accepted 10 January 2012
Available online 13 January 2012

Keywords:
Mesoporous silica nanosphere
Anthracene
Cu^{2+}
Sensitivity
Selectivity
Reversibility

ABSTRACT

Monodisperse mesoporous silica nanosphere (MSN) modified with anthracene derivative, 2-(3-(triethoxysilyl) propylamino)-N-(9-anthryl methyl) acetamide (SGAAn) has been fabricated as a fluorescent sensor (SGAAn-MSN) for the detection of metal ions, which shows an exclusive selectivity to Cu^{2+}. Compared with SGAAn, SGAAn-MSN presents a higher sensitivity to Cu^{2+}. The loading amount of SGAAn in MSN has a great influence on the detection sensitivity of SGAAn-MSN, which varies with the local concentration and accessibility of SGAAn in the pore channel of MSN. Interference studies indicate that the addition of other metal ions such as Ag^{+}, Cd^{2+} and Pb^{2+} has a negligible effect on the selectivity of SGAAn-MSN to Cu^{2+}. The possible mechanism for the sensing behavior of SGAAn-MSN to Cu^{2+} is proposed based on the relation between fluorescence quench degree and Cu^{2+} concentration.

1. Introduction

The pollution caused by heavy metal ions is extremely harmful to the environment and human health [1]. Heavy metal ions such as Pb^{2+}, Hg^{2+} and Ag^{+} should not even exist in human beings at all, which may cause great poisonous effect even with trace amount [2,3]. Others like Zn^{2+}, Fe^{3+} and Cu^{2+} are involved in the bioactivity of human beings, but may also cause toxicity when exceeding the limit [4–6].

Heavy metal ions entering into the river and soil caused by the exploitation and smelting may gradually accumulate in human beings after they are involved in bioactivities, so, it is very important to detect the trace of heavy metal ions. Currently, the commonly used techniques for metal ions detection include atomic absorption spectrophotometry, X-ray fluorescence spectrophotometry, inductively coupled plasma atomic emission spectrometry and electrochemical method [7,8]. Compared with the above methods, fluorescence analysis is more popular due to its real-time operation, efficiency and convenience. Moreover, the precise information including ions valence or molecule structure can also be read out through the variation of fluorescence spectra.

A metal ion fluorescent sensor generally composes of a recognition site designed to bind the target ion and a readout system, which is often a fluorophore. It is known many metal ions tend to be bound by chelate groups composed of N, O and S [9]. Fluorescent sensors generally show good selectivities to metal ions, which are determined by binding affinity and size matching between chelate groups and metal ions [10]. However, the detection sensitivity of traditional fluorescent sensor for metal ions is often not high enough to satisfy the increasing application requirement. Currently, detection of tiny metal ions often needs an enriching procedure, which is troublesome and inefficient. With the development of nanoscience, the application of nanomaterials for metal ions detection becomes more and more interesting and has caused tremendous attention since this kind of composite shows a high sensitivity to biomolecules, poisonous gas and heavy metal ions [11–20]. However, fluorescent sensor for the detection of tiny metal ions is still in great need due to the less effective performance of most sensors in the new emerging application fields such as ions sensing and imaging in biosystem.

Mesoporous silica material reported in 1992 is a good solid base for the fabrication of organic–inorganic hybrid materials by introducing dye molecules into the pore framework or the pore channel due to its abundant surface hydroxyl groups and open pore system [21]. The hybrid composite may present novel and interesting properties compared with the corresponding dye molecules. Moreover, due to its nontoxicity and biocompatibility, composite based on mesoporous silica has good potential applications in biosystem. However, the failure to obtain discrete or non-aggregated silica nanoparticles has obstructed its application in the biosystem since monodisperse mesoporous silica nanomaterial is a more suitable alternative used as *in vivo* fluorescence imaging

* Corresponding authors. Tel./fax: +86 21 64252062.
E-mail addresses: jlzhang@ecust.edu.cn (L. Wang), wlz@ecust.edu.cn (J. Zhang).

0143-7208/$ – see front matter © 2012 Elsevier Ltd. All rights reserved.
doi:10.1016/j.dyepig.2012.01.004

medium, efficient ions remover and drug releasing medium [22–24], which may present more powerful characteristics and potential application than other nano solid platform when it is used as a fluorescent sensor.

Cu^{2+} is an essential element for human beings and a disorder of Cu^{2+} metabolism is closely associated with many severe neurological diseases such as Menkes and Wilson disease, Alzheimer's disease, familial amyotrophic lateral sclerosis and prion disease [25]. The maximum permissible limit of copper ion discharged in water for most of countries around the world is 3.0 ppm. However, the pollution situation caused by copper ion is still very severe and it has been intensively studied as the detection target for many fluorescent sensors [26–28]. This paper presents a novel Cu^{2+} fluorescent sensor based on mesoporous silica nanosphere by using anthracene as the readout unit. We chose anthracene and introduced it into the pore channel of mesoporous silica nanosphere since this kind of polycyclic aromatic hydrocarbon has high fluorescence quantum quantity and stable fluorescence signal, which is an ideal report unit for fluorescent sensor. It is known Cu^{2+} tends to interact with peptide and heterocyclic ring by coordinating with N, O or S atom [29], so we modified anthracene with groups composed of amine and amide before it is anchored on the pore surface. The selectivity and sensitivity of this composite to Cu^{2+} was carefully studied by fluorescence spectra. The sensing mechanism of this nanocomposite was proposed based on the relation between the fluorescence intensity and Cu^{2+} concentration.

2. Experimentals

2.1. Materials

Chemicals for reactions were purchased from Sigma–Aldrich and are of A.R. grade. Solvents used in silica gel chromatography including ethyl acetate (EA) and petroleum ether (PE) were purchased from Sinopharm Chemical Reagent Co. Ltd. NMR solvent was purchased from J&K Chemical Ltd. All starting materials and solvents were used as received without further purification.

2.2. Preparation

The synthesis of target compound **5**, 2-(3-(triethoxysilyl) propylamino)-N-(9-anthrylmethyl) acetamide (SGAAn) was achieved by the route outlined in Scheme 1.

2.2.1. Synthesis of 9-azidomethylanthracene (*2*)

Compound **1** (1.54 g, 7.40 mmol) was dissolved in CH_2Cl_2 (30 mL), and then $SOCl_2$ (810 μL, 11.10 mmol) was added at 0 °C. After 1 h, the solvent was removed under vacuum. The resultant residue was dissolved in DMF (10 mL), and sodium azide (777 mg, 11.95 mmol) was added. The reaction mixture was heated for 1 h at 50 °C, cooled to room temperature and diluted with 50 mL water. After extraction with EA, the organic layer was washed with brine, dried over $MgSO_4$ and concentrated under vacuum. Purification of the residue by silica gel chromatography (EA/PE = 1/19) gives **2** as a yellow solid (1.669 g, 97% yield). ^{1}H NMR (400 MHz $CDCl_3$) δ 5.33 (s, 2H), 7.50 (t, 2H, J = 8 Hz), 7.59 (t, 2H, J = 8 Hz), 8.06 (d, 2H, J = 8.4 Hz), 8.28 (d, 2H, J = 8.8 Hz), 8.50 (s, 1H); ^{13}C NMR (100 MHz CDCl3) δ 46.39, 123.54, 125.23, 126.87, 129.02, 129.33, 130.74, 131.41; EI found 233.1 $[M]^{\cdot+}$ calculated for $C_{15}H_{11}N_3$: 233.1.

2.2.2. Synthesis of 9-aminomethylanthracene (*3*)

The suspension of compound **2** (0.4 g, 1.93 mmol) and 10% Pd/C (204 mg) in EA (20 mL) sealed in a bottle was charged with N_2 for 3 times and H_2 for 4 times, and then put under H_2 for 4 h. The completion of the reaction was determined by thin layer chromatography (TLC). The reaction was filtered and washed with EA. The filtrate was concentrated to give product **3** as a pale yellow solid (391 mg, 98% yield). ^{1}H NMR (400 MHz $CDCl_3$) δ 1.69 (s, 2H), 4.82 (s, 2H), 7.47 (t, 2H, J = 7.4 Hz), 7.55 (t, 2H, J = 8 Hz), 8.02 (d, 2H, J = 8.4 Hz), 8.33 (d, 2H, J = 8.8 Hz); 8.40 (s, 1H); ^{13}C NMR (100 MHz $CDCl_3$) δ 38.24, 123.72, 125.01, 126.19, 126.97, 129.33, 131.72; EI found 207.1 $[M]^{\cdot+}$ calculated for $C_{15}H_{13}N$:207.1.

2.2.3. Synthesis of N-(9-anthylmethyl)-2-chloro acetamide (*4*)

Compound **3** (414 mg, 2 mmol) and triethylamide (0.3 mL) were dissolved in dichloromethane (20 mL) at 0 °C. Then chloroacetyl chloride (0.17 mL) was added. The mixture was warmed to room temperature and allowed to react overnight. The solvent was evaporated under vacuum. The crude product was further purified by silica gel chromatography (PE/EA = 3). A yellow solid was obtained (416 mg, Yield: 74%). ^{1}H NMR (400 MHz $CDCl_3$) δ 4.10 (s, 2H), 5.49 (d, 2H, J = 5.2 Hz), 6.72 (s, 1H), 7.52 (t, 2H, J = 7.2 Hz), 7.60 (t, 2H, J = 8.0 Hz), 8.06 (d, 2H, J = 8.4 Hz), 8.27 (d, 2H, J = 9.2 Hz), 8.51 (s, 1H); ^{13}C NMR (100 MHz $CDCl_3$) δ 36.45, 42.50, 123.50, 125.30, 127.00, 128.62, 129.36, 130.43, 131.49; ESI found 284.1 $[M+H]^+$ calculated for $C_{17}H_{14}ClNO$: 283.08.

2.2.4. Synthesis of 2-(3-(triethoxysilyl) propylamino)-N-(9-anthrylmethyl) acetamide(5, SGAAn)

A mixture of **4** (309 mg, 1.40 mmol) and K_2CO_3 (261 mg, 1.91 mmol) in CH_3CN (10 mL) was added to a solution of **4** (360 mg, 1.27 mmol) in CH_3CN (20 mL) and the mixture was refluxed overnight under N_2 protected. The solvent was evaporated under vacuum and the crude product was purified by silica gel

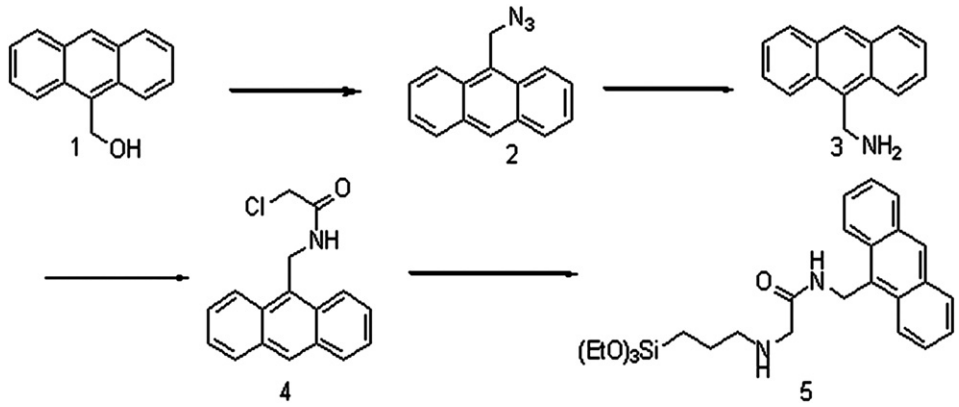

Scheme 1. Synthetic route for SGAAn.

chromatography (EA) to give **5** as yellow oil. ^{1}H NMR (400 MHz $CDCl_3$) δ 0.37 (t, 2H, $J = 8$ Hz), 1.13 (t, 9H, $J = 7.2$ Hz), 1.30–1.40 (m, 2H), 1.61 (s, 1H), 2.43 (t, 2H, $J = 7.2$ Hz), 3.27 (s, 2H), 3.67 (q, 6H, $J = 6.8$ Hz), 5.42 (d, 2H, $J = 5.2$ Hz), 7.47 (t, 3H, $J = 7.6$ Hz), 7.55 (t, 2H, $J = 8$ Hz), 7.80 (d, 2H, $J = 8.4$ Hz), 8.30 (d, 2H, $J = 8.4$ Hz), 8.44 (s, 1H); ^{13}C NMR (100 MHz $CDCl_3$) δ 7.61, 18.23, 23.13, 35.47, 152.28, 52.58, 58.29, 123.91, 125.16, 126.60, 128.00, 129.18, 130.37, 131.51, 171.61; ESI found 469.1 $[M+H]^+$ calculated for $C_{26}H_{36}N_2O_4Si$: 468.24.

2.2.5. Synthesis of SGAAn modified mesoporous silica nanosphere (MSN)

Mesoporous silica nanosphere (MSN) was prepared according to a method reported in our previous publication [30]. The preparation of dye modified MSN was as follows: 100 mg dried MSN was first suspended in 30 mL of anhydrous acetonitrile in a round bottomed flask connected to a Dean-stark apparatus under nitrogen, and then 14 mg SGAAn was added. The mixture was stirred for 24 h at 100 °C. The SGAAn modified MSN was collected by filtration and repeatedly washed with anhydrous acetonitrile, dichloromethane and ethanol under ultrasonic condition. Unreacted organic material was completely removed by monitoring the absorbance of the washing liquid. The ultimate powder was dried under vacuum and named as SGAAn-MSN. The actual loading amount of SGAAn per gram of SGAAn-MSN was calculated to be 1.26×10^{-4} mol according to the UV–vis absorption spectra of the filtration eluent. The following study concerned with SGAAn-MSN without specific explanation refers to sample loaded with 1.26×10^{-4} mol SGAAn per gram of SGAAn-MSN. Moreover, another two samples loaded with 0.96×10^{-4} and 2.31×10^{-4} mol SGAAn per gram of SGAAn-MSN were also prepared to study the influence of SGAAn amount to the detection sensitivity.

2.2.6. Relations between pH value and fluorescence of SGAAn-MSN

The pH value of SGAAn-MSN solution was adjusted using 2 M NaOH aqueous solution. The specific operation was as follows: (1) Preparation of a EtOH–Water solution of SGAAn-MSN with pH = 3 (30% EtOH, 100 mL, 10^{-5} M for SGAAn); (2) 100 μL Cu^{2+} (2×10^{-2} M) was added to the SGAAn-MSN solution and the fluorescent intensity was recorded; (3) The pH value of the above complex solution was adjusted from 3 to 12 using 2 M NaOH solution and the fluorescent intensity change was recorded.

2.2.7. Reversibility of SGAAn-MSN as Cu^{2+} fluorescent sensor

The chelate agent used in this experiment was a solution of EDTA–2Na (0.1 M). The whole process for the investigation of reversibility was as follows: (1) Preparation of a EtOH–Water solution of SGAAn-MSN (30% EtOH, 100 mL, 10^{-5} M SGAAn); (2) excessive amount of Cu^{2+} (2×10^{-4} mol) was added to the solution to adequately coordinate with SGAAn; (3) 5×10^{-4} mol EDTA-2Na was added to the above complex solution to replace SGAAn. The fluorescence intensities of the above solutions for each step were recorded. SGAAn-MSN was recovered by centrifuging and washed with a tris–HCl (0.01 M) solution (water, pH = 7.10) and distilled water. The above process was totally repeated for 4 circles.

2.3. Characterization

X-ray powder diffraction (XRD) patterns of all samples were recorded on Rigaku D/MAX-2550 diffractometer using Cu Kα radiation on wavelength of 0.154 nm, operated at 40 kV and 100 mA. UV–visible absorbance spectra were obtained with a scan UV–visible spectrophotometer (Varian, Cary 500). The fluorescence spectra of all samples were recorded with Cary Eclipse fluorescence spectrophotometer. Scanning electron microscopy (SEM) images were obtained with a JEOL JSM-6360LV microscope at an accelerating voltage of 15 kV. Transmission electron microscopy (TEM) images were collected on a JEOL JEM 2010F, electron microscope operated at an acceleration voltage of 200 kV. 1H and 13C NMR spectra were obtained on a Bruker AVANCE DMX500 spectrometer in $CDCl_3$ with tetramethylsilane (TMS) as internal standard. ICP-AES data were recorded on Varian-710-ES instrument. Electron impact mass spectra were recorded on an Agilent 5973N MSD instrument, and ESI mass spectra were recorded on Agilent 11100-Finnigan instrument.

3. Results and discussion

3.1. Mesoporous structure

Fig. 1 shows the SEM and TEM images of mesoporous silica nanoparticles. It is obvious that these particles are spherical and highly dispersive. The approximately average particle size is about 125 nm as seen from TEM by measuring over 100 particles. The pore channel is aligned from the center to the fringe, which is an ideal structure for the access and dispersion of guest molecules. As seen from Fig. 2(a), sample without dye modification shows a clear peak at $2\theta = 1.53$, which further verifies the mesoporous characteristic of MSN. However, it is obvious that the introduction of dye molecules into the pore channel makes some deterioration of pore ordering since the peak intensity is largely decreased, which is further approved by N_2 adsorption–desorption experiment. Fig. 2(b) shows the N_2 adsorption–desorption isotherms and

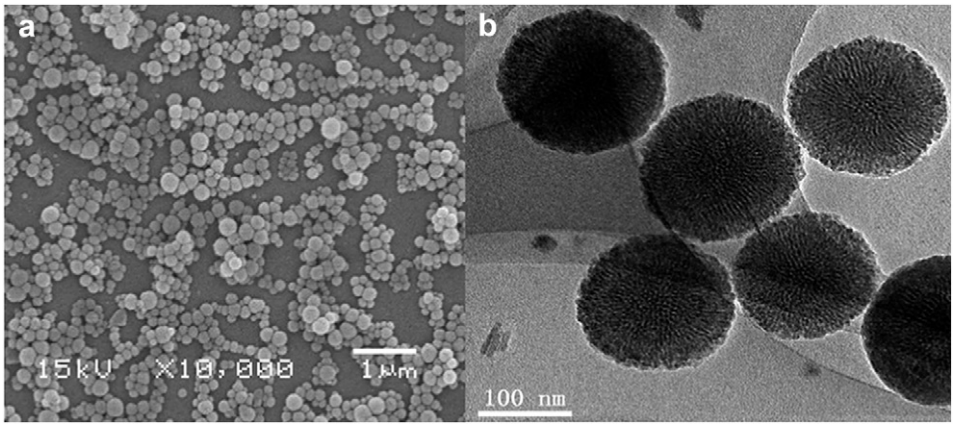

Fig. 1. SEM (a) and HRTEM (b) images of MSN.

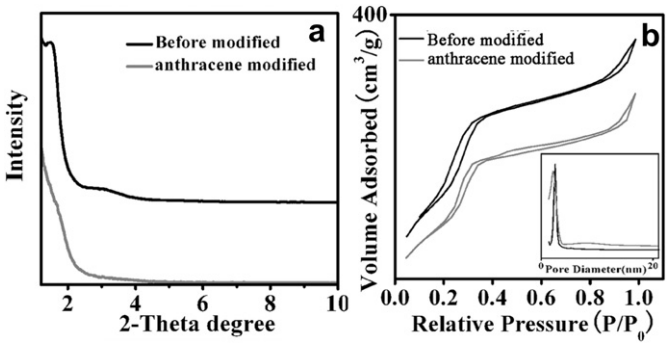

Fig. 2. XRD patterns (a) and N_2 absorption/desorption isotherms (distribution of pore size, insert) of MSN before (black) and after (gray) loaded with dye molecules.

distribution of pore size (inset b) of samples before and after dye loading, which both exhibit a type IV isotherm typical for mesoporous material. It can be seen that the introduction of dye molecules into MSN decreases the N_2 adsorption ability of MSN. The BET surface area decreases from 631 to 497 $m^2\ g^{-1}$, the pore volume calculated by BJH method decreased from 0.526 to 0.472 cc g^{-1} and the pore size calculated by BJH method show small decrease from 2.50 to 2.49 nm.

3.2. Optical properties

Fig. 3(a) shows the absorption spectrum of SGAAn and solid diffuse reflection spectrum of SGAAn-MSN. It is obvious that both SGAAn and SGAAn-MSN show a maximum absorption peak at about 254 nm. Therefore, the incorporation of SGAAn in the pore channel does not change its absorption property, which indicates the preserving of molecule structure of anthracene after reaction with surface silanol groups. The average dye molecule numbers doped into each MSN particle is calculated as follows: First, the standard curve of absorbance versus concentration for SGAAn was plotted; then the loading amount of SGAAn molecules per gram of MSN was calculated from the maximum absorption intensity of filtrated SGAAn solution; Subsequently, the numbers of per gram of MSN was determined by drying and weighing a certain volume of nanoparticle solution. Ultimately, the dye molecule numbers per nanoparticle is calculated to be about 2000. The local concentration of dye molecules in one silica nanosphere is calculated to be about 3×10^{-3} M. The fluorescence spectra of SGAAn and SGAAn-MSN solution are shown in Fig. 3(b). The total dye concentration for SGAAn and SGAAn-MSN in the solution using 30% EtOH and 70% water as solvents is fixed as 10^{-5} M. EtOH in SGAAn solution is used to relieve the hydrolysis of alkoxyl silane groups of SGAAn during fluorescence analysis, and to keep the same with SGAAn, EtOH was also added into the SGAAn-MSN solution although the alkoxyl silane groups has already reacted with the silanol groups on the pore surface. As seen from Fig. 3(b), SGAAn-MSN shows similar fluorescence spectrum with SGAAn but has lower peak intensity. Nevertheless, it seems that SGAAn-MSN still preserves observable fluorescence intensity although SGAAn molecules anchored in MSN has a high local concentration (3×10^{-3} M) in the pore channel. Generally, dye molecules in the homogeneous solution system will encounter severe self-quench in the high concentration state. Moreover, it is known the packing of dye molecules in the solid base will also cause the fluorescence quench. The relieved fluorescence quench of SGAAn-MSN can be explained as follows: MSN has abundant pore channel and surface silanol groups. SGAAn molecules can be highly dispersed into the pore channel of MSN and covalently fixed in the different location of pore surface by reaction

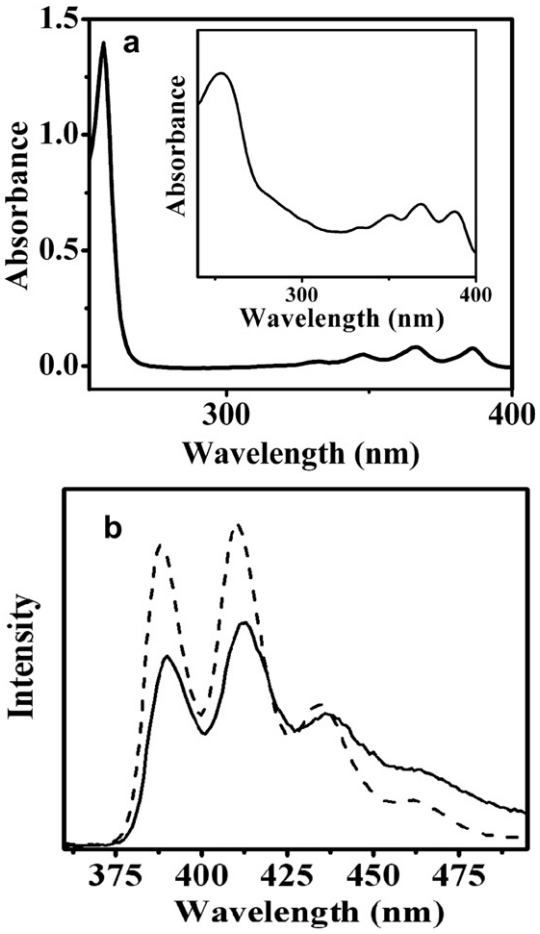

Fig. 3. (a) Absorption and solid diffuse reflection spectra of SGAAn and SGAAn-MSN (inset) and (b) Fluorescence spectra of SGAAn (Dash) and SGAAn-MSN (solid). The solution composes of EtOH and water with a ratio of 3:7.

with silanol groups, which means the mobility and rotation of SGAAn is restricted in a fixed area. Therefore, the molecule collision can be effectively avoided even dye molecules are densely located in MSN, and the generally observed severe fluorescence quench in dye solution with high concentration can be much reduced.

3.3. Influence of pH value to the fluorescence of SGAAn-MSN solution

Fig. 4 shows the relation between pH value and the fluorescence intensity of SGAAn-MSN (10^{-5} M) in the presence of Cu^{2+} (2×10^{-5} M). It can be found from Fig. 4 that the fluorescence intensity of SGAAn-MSN has different responsive behaviors in different pH ranges, which first slowly increases with the increasing pH value from 3 to 6, especially in the range of 5–6, then almost remains unchanged in the range of 6–9, and finally abruptly increases with the increasing pH value from 9 to 12. The small increase of the fluorescence intensity with the increasing pH value from 3 to 6 should be attributed to the deprotonation of imine by reducing the electron transfer fluorophore to protonated N. The significant increase of the fluorescence intensity with the increasing pH value from 9 to 11 should be attributed to the displacing of Cu^{2+} from the complex, leading to the recovery of the fluorescence of SGAAn. From Fig. 4 we can conclude that the coordination between SGAAn-MSN and Cu^{2+} is stable in the pH range of 7–9. Therefore, 0.05 M of HEPES buffer solution (pH = 7) was selected for the subsequent studies.

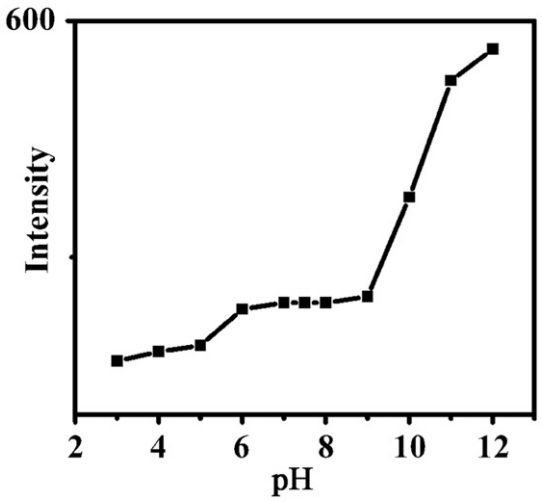

Fig. 4. Relation between pH value and fluorescence intensity of SGAAn-MSN (10^{-5} M) in the presence of Cu^{2+} (2×10^{-5} M).

3.4. Selectivity

Fig. 5 shows the fluorescence spectra of SGAAn and SGAAn-MSN with dye concentration of 10^{-5} M in the presence of various metal ions. It can be found that the fluorescence intensities of SGAAn and SGAAn-MSN considerably decrease in the presence of Cu^{2+} with 10^{-4} M. However, the addition of other metal ions such as Zn^{2+}, Fe^{3+}, Pb^{2+} and Ag^{+} with the same concentration does not trigger obvious fluorescence change of the sensor, which well illustrates the selectivity of the above sensors to Cu^{2+}. Generally, the fluorescence quench efficiency is determined by the coordinating and size matching state between metal ions and the recognition site of sensor molecule as well as the quenching ability of ions. It is well known that ions such as Zn^{2+}, Cu^{2+}, Pb^{2+} and Ag^{+} have high thermodynamic affinity for chelate ligand composed of N, O and S and fast metal-to-ligand binding kinetics. However, as seen from Fig. 5, only Cu^{2+} cause obvious fluorescence quench of anthracene. It is because Cu^{2+} with d^9 electronic configuration has good ability to accept electron. The radiationless deactivation of the excited state of the fluorophore by Cu^{2+} can take place by means of either an energy transfer mechanism occurring by electron exchange with an unpaired d orbital of Cu^{2+} or an anthracene-to-Cu^{2+} electron transfer process [9]. Therefore, the effective fluorescence quench can occur when Cu^{2+} coordinates with the recognition site of sensor molecule. Different from Cu^{2+}, ions such as Zn^{2+} and Cd^{2+} with d^{10} electronic configuration and no unpaired electron has poor ability to accept electron from anthracene, leading to the negligible influence to the fluorescence. Ions such as Ag^{+} also have no influence on the fluorescence of anthracene, which may be due to the inefficient coordination between Ag^{+} with large size and chelate group. Except for Cu^{2+}, Pb^{2+} shows more obvious influence to the fluorescence of anthracene than other metal ions, which should be attributed to the heavy atom effect. The interference of different metal ions to Cu^{2+} was also studied as seen from Fig. 6. It is obvious that the addition of other metal ions in the presence of Cu^{2+} has a negligible influence on the fluorescence intensity of SGAAn and SGAAn-MSN, which indicates the sensor presented here has high anti-interference ability.

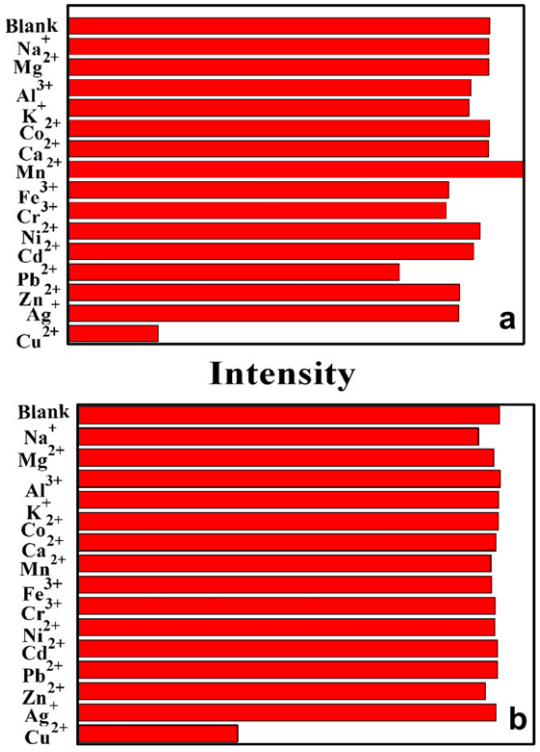

Fig. 5. Fluorescence spectra of SGAAn (a) and SGAAn-MSN (b) in the presence of various metal ions (10^{-4} M) excited with 254 nm. 0.05 M HEPES buffer solution was used to keep pH at 7.0. The solution composes of EtOH and water with a ratio of 3:7.

3.5. Sensitivity

The contact-time between Cu^{2+} and SGAAn-MSN is very short, which is only about 4–5 s. Here, the detection sensitivities of SGAAn and SGAAn-MSN were mainly evaluated by using 10% decrease of the initial fluorescence intensity of SGAAn and SGAAn-MSN in the presence of Cu^{2+}. As shown in Fig. 7, the obvious 10%

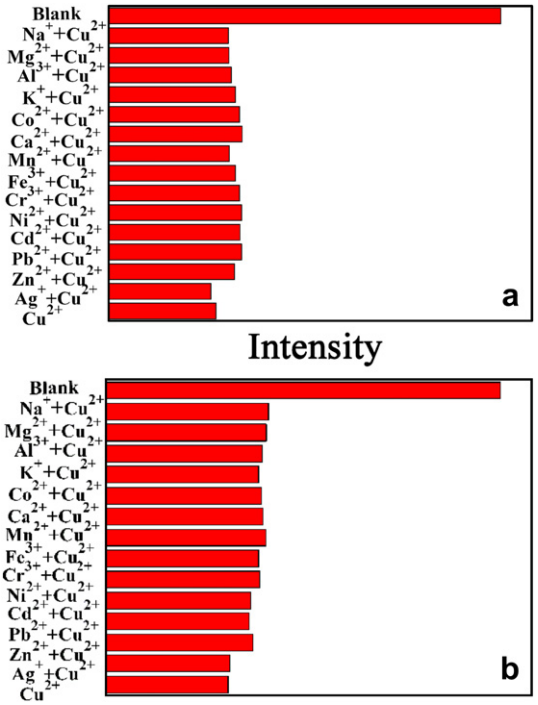

Fig. 6. Fluorescence intensity of SGAAn (a) and SGAAn-MSN (b) (10^{-5} M) in the presence of various metal ions (10^{-4} M) and Cu^{2+} (10^{-4} M).

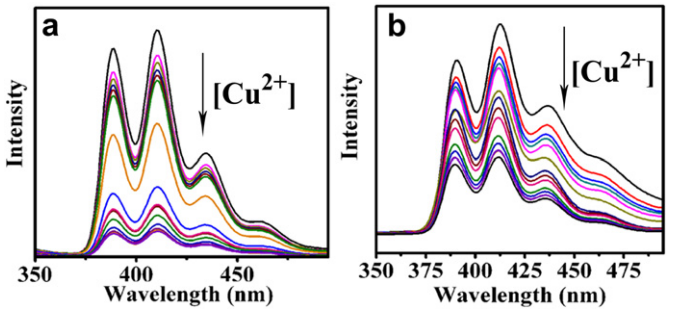

Fig. 7. Fluorescence spectra of SGAAn (a) and SGAAn-MSN (b) with different amount of Cu^{2+} (a: from the top of 4×10^{-6} to the bottom of 10^{-3} M; b: from the top of 5×10^{-8} to the bottom of 10^{-4} M).

decrease of the fluorescence intensity is observed when the concentration of Cu^{2+} reaches to 10^{-6} M for SGAAn and 5×10^{-8} M for SGAAn-MSN, which indicates the sensitivity of SGAAn-MSN is significantly improved compared with SGAAn. The detection limit of SGAAn-MSN was calculated according to equation (1), where x_{min} is the minimal analytical signal that can be detected, $\bar{x}_0$ is the average fluorescence intensity of blank SGAAn-MSN solution under the same condition, K is the confidence level and S_0 is the standard deviation of blank. Here, $\bar{x}_0$ and S_0 are calculated to be 497 and 4.5, respectively. x_{min} is calculated to be 483.5 by setting the K value as generally used 3, which corresponds to 2×10^{-8} M Cu^{2+}. Therefore, the detection limit of SGAAn-MSN for Cu^{2+} is 2×10^{-8} M.

$$x_{min} = \bar{x}_0 + KS_0 \quad (1)$$

The sensitivity of SGAAn-MSN loaded with different amount of SGAAn to Cu^{2+} was also compared. As seen from Fig. 8(a), the actual loading amounts of SGAAn per gram of MSN for samples a, b and c is 0.96, 1.26 and 2.31 $\times 10^{-4}$ mol/g, respectively. It is obvious that sample b shows the best sensitivity. It indicates that too much or too less loading amount leads to the decrease of sensitivity, which can be explained as follows: Dye molecules introduced into the pore channel may lead to some deterioration of mesoporous structure and the obstruction of pore channel, which is approved by N_2 absorption–desorption isotherms. Fig. 8(b) shows the N_2 absorption–desorption isotherms of MSN with various loading amounts of SGAAn. It can be seen that the N_2 adsorption ability of SGAAn-MSN decreases with the increasing loading amounts of dye molecules because the relative pressure becomes lower. The BET surface area decreases from 497, 432 to 368 $m^2\ g^{-1}$ and the averagepore size calculated by BJH method decreases from 2.49, 2.11 to 1.76 nm for sample a, b and c. Cu^{2+} can not well interact with dye molecules if the pore channel is severely obstructed when too much dye molecules are introduced. However, too less dye molecule is also disadvantageous to the sensitivity since the local concentration of dye molecules around Cu^{2+} in the pore channel is low. Furthermore, to study the removing ability of SGAAn-MSN for Cu^{2+}, we evaluated the removing efficiency of sample b for Cu^{2+} by ICP-AES. A Cu^{2+} solution of 3×10^{-6} M (50 mL, 0.19 ppm) was treated with 40 mg of sample b (1×10^{-4} M SGAAn) for 1 h and then the nanoparticle was filtrated. The residual Cu^{2+} in the filtrate is 0.02 ppm determined by ICP-AES, which means that about 90% of Cu^{2+} in aqueous solution is adsorbed by SGAAn-MSN. Therefore, SGAAn-MSN is a promising functional material for the use in the removal of Cu^{2+} from polluted water.

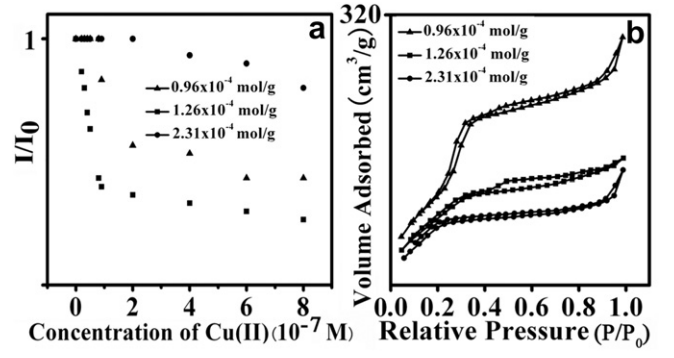

Fig. 8. Sensitivities and N_2 adsorption/desorption isotherms of SGAAn-MSN loaded with different amount of anthracene.

3.6. Detection reversibility of SGAAn-MSN

To evaluate the sensing reversibility of SGAAn-MSN to Cu^{2+}, the fluorescence changing of SGAAn-MSN coordinating with Cu^{2+} was repeatedly studied for 4 cycles by using EDTA-2Na (10^{-3} M) as the chelate agent and the results are shown in Fig. 9. As seen from Fig. 9, the fluorescence of SGAAn-MSN can almost be totally recovered after the addition of EDTA-2Na, which shows good response to the further addition of Cu^{2+} for each cycle. The above result means SGAAn-MSN possesses an excellent reusability and stability for the sensing of Cu^{2+}.

3.7. Mechanism

To investigate the coordination information between Cu^{2+} and SGAAn, the titration curve of SGAAn (10^{-5} M, Fig. 10) in the presence of various amount of Cu^{2+} was plotted. According to the inflection point, SGAAn molecules and Cu^{2+} form a 1:1 complex. The fluorescence quenched by further addition of Cu^{2+} above 10^{-5} M becomes moderate, which should be caused by molecule collision between fluorophore and Cu^{2+}. Differently, quench caused by the complex formation is named as static quench, which is more effective and can be described as Stern–Volmer equation, $I_0/I = 1 + K_{SV}[Q]$, where $[Q]$ is the Cu^{2+} concentration, K_{SV} is the Stern–Volmer quenching constant, and I and I_0 are fluorescence intensities of SGAAn in the presence and absence of Cu^{2+}, respectively. As shown in the insert of Fig. 10, a good linearity is observed when the concentration of Cu^{2+} is below 10^{-5} M and K value is found to be $1.6 \times 10^5\ M^{-1}$.

Since Cu^{2+} and SGAAn form a 1:1 complex and Cu^{2+} desires a square planar geometry when it is coordinated, we infer that the

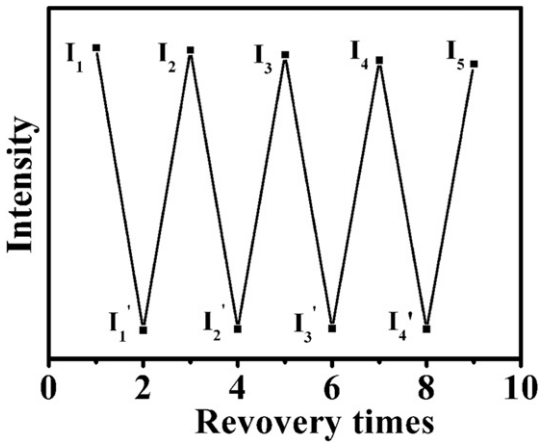

Fig. 9. Reversibility of the sensing response of SGAAn-MSN (10^{-6} mol SGAAn) to Cu^{2+} (2×10^{-4} mol). $I_1 \sim I_5$ corresponds to the fluorescence intensity of SGAAn-MSN after the displacing of SGAAn from the Cu^{2+} complex by EDTA–2Na (5×10^{-4} mol). $I_1' \sim I_4'$ corresponds to the fluorescence intensity of SGAAn-MSN coordinated with Cu^{2+}.

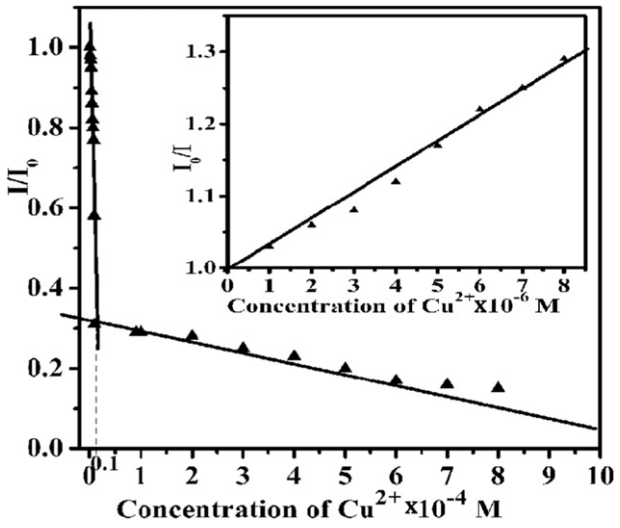

Fig. 10. Titration curve and Stern–Volmer plot (inset) of SGAAn (10^{-5} M) treated with Cu^{2+}.

two nitrogen atoms on SGAAn, together with silanol oxygen on the pore surface of MSN provide ligands to coordinate with Cu^{2+} (Fig. 11), leading to the fluorescence quench of SGAAn-MSN. The Stern–Volmer plot for SGAAn-MSN in the presence of various amount of Cu^{2+} is shown in Fig. 12. As seen from Fig. 12(a), the addition of tiny amount of Cu^{2+} into SGAAn-MSN (1.26×10^{-4} mol/g) solution containing 10^{-5} M SGAAn leads to much more obvious fluorescence quench than SGAAn solution with the same concentration. I_0/I linearly increases with the increasing Cu^{2+} concentration in the range of $0–10^{-7}$ M and the corresponding K_{SV} value is 1.24×10^7 M^{-1} (Fig. 12a (inset)). The improved quench constant can be attributed to the following reasons: (1) The opening pore channel and negatively charged pore surface of MSN make Cu^{2+} more accessible to the dye molecules; (2) The dye molecules anchored in the pore channel are fixed and well dispersed. The local concentration of dye molecules in one mesoporous silica nanoparticle is much higher than the total dye concentration in solution. This arrangement avoids the molecule collision between dye molecules and improves the contact possibility between dye and metal ions. When Cu^{2+} enters into the pore channel, it is surrounded by anthracene in a restricted space of nanoporous channel, leading to more effective energy or electron transfer. Therefore, the fluorescence is more efficiently quenched even the total concentration of anthracene in solution is low. For the homogeneous SGAAn solution, unless the quencher concentration is very high, significant quenching requires fast diffusion to bring molecules into contact. The increasing of dye concentration may also lead to the situation that dozens of times of SGAAn molecules center around Cu^{2+} in a nanometer-sized circle region when tiny amount of Cu^{2+} is added into the solution. However, an over high concentration of dye molecules often results in a severe self-quench of fluorescence

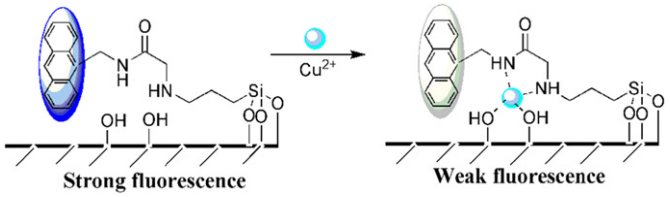

Fig. 11. Binding between Cu^{2+} and ligands and the turn-off fluorescence response of SGAAn-MSN.

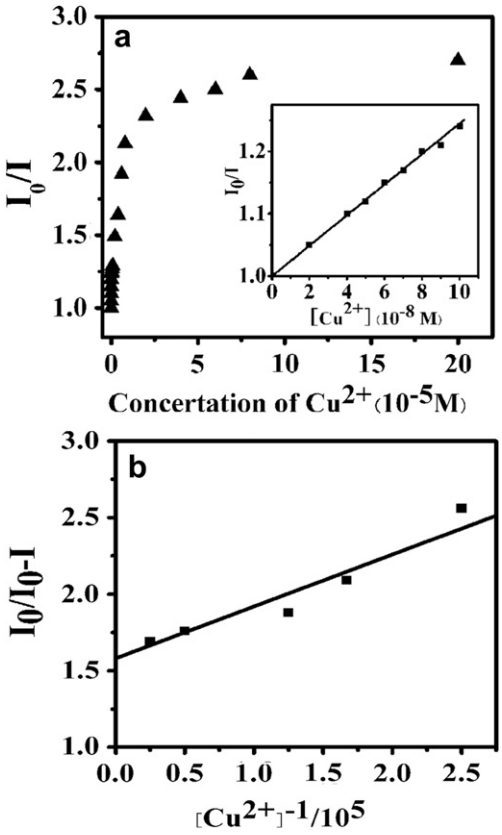

Fig. 12. (a) Stern–Volmer plot for SGAAn-MSN; (b) modified Stern–Volmer plots for two populations of fluorophores in SGAAn-MSN.

since dye molecules are free in solution and these molecules will inevitably encounter frequent intermolecular collisions.

Moreover, the Stern–Volmer plot of the above SGAAn-MSN solution shows an unusually severe deviation from linearity toward the *x*-axis when only half of fluorescence intensity is quenched. Generally, a linear Stern–Volmer plot is indicative of a single class of fluorophore, all equally accessible to quencher. If two fluorophore populations are present and one class is not accessible to quencher, the Stern–Volmer plots will deviate from linearity toward the *x*-axis. This result is frequently found for the quenching of tryptophan fluorescence in proteins by polar or charged quenchers [9]. These molecules do not readily penetrate the hydrophobic interior of proteins, and only those tryptophan residues on the surface of the protein are quenched. For the dye modified mesoporous structure, the dye anchored in the pore channel may lead to the pore narrowing and even obstruction. Therefore, dye molecules located in the interior center of mesoporous sphere become inaccessible, which means two groups of dye molecules divided into the accessible and the inaccessible lead to the deviation of Stern–Volmer plot to *x*-axis.

$$\frac{I_0}{I_0 - I} = \frac{1}{f_a K_a [Q]} + \frac{1}{f_a} \tag{2}$$

The accessible dye molecules in the pore channel can be calculated according to equation (2) [31], where K_a is the Stern–Volmer quenching constant of the accessible fraction, f_a is the fraction of the initial fluorescence that is accessible to quencher and $[Q]$ is the concentration of quencher. A plot of $I_0/(I_0 - I)$ versus $1/[Q]$ yields $1/f_a$ as the intercept. As seen from Fig. 12(b), the f_a value of the above sample is about 0.6 calculated from the intercept, which means more than half of dye molecules are accessible to Cu^{2+}.

4. Conclusions

Monodisperse mesoporous silica nanoparticles modified with anthracene derivative present a good selectivity and a high sensitivity to Cu^{2+}. The presence of other metal ions such as Zn^{2+}, Cd^{2+}, Fe^{3+}, Pb^{2+} and Ag^{+} has little influence on the selectivity of Cu^{2+}. The sensitivity of this nanocomposite to Cu^{2+} is determined by the local concentration and accessibility of dye molecules in the pore channel. The improved sensitivity of the nanocomposite is due to the high local concentration of dye molecules in the pore channel with less self fluorescence quench caused by molecule collision.

Acknowledgments

This work has been supported by National Nature Science Foundation of China (21007016 and 20977030), the Project of International Cooperation of the Ministry of Science and Technology of China (2011DFA50530), Science and Technology Commission of Shanghai Municipality (11142201100) and the Fundamental Research Funds for the Central Universities.

References

[1] Hosono T, Su CC, Siringan F, Onodera SC. Effects of environmental regulations on heavy metal pollution decline in core sediments from Manila Bay. Marine Pollut Bull 2010;60:780–5.
[2] Nriagu JO. A silent epidemic of environmental metal poisoning. Environ Pollut 1988;50:139–61.
[3] Clarkson TW, Magos L, Myers GJ. The toxicology of mercury – current exposures and clinical manifestations. N Engl J Med 2003;349:1731–7.
[4] Berg JM, Shi Y. The galvanization of biology: a growing appreciation for the roles of Zinc. Science 1996;271:1081–5.
[5] Waggoner DJ, Bartnikas TB, Gitlin JD. The role of copper in neurodegenerative disease. Neurobiol Dis 1999;6:221–30.
[6] Weizman H, Ardon O, Mester B, Libman J, Dwir O, Hadar Y, et al. Fluorescently-labeled ferrichrome analogs as probes for receptor-mediated microbial iron uptake. J Am Chem Soc 1996;118:12368–75.
[7] Manjusha R, Dash K, Karunasagar D. UV-photolysis assisted digestion of food samples for the determination of selenium by electrothermal atomic absorption spectrometry. Food Chem 2007;105:260–5.
[8] He Q, Chang XJ, Huang XP, Hu Z. Silica gel surface-imprinted solid-phase extraction of Zr (IV) from aqueous solutions. Microchim Act 2008;160:147–52.
[9] Fabbrizzi L, Licchelli M, Pallavicini P. Transition metals as switches. Acc Chem Res 1999;32:846–53.
[10] Kim JS, Quang DT. Calixarene-derived fluorescent probes. Chem Rev 2007; 107:3780–99.
[11] Lee HY, Son HJ, Lim JM, Oh JM, Kang DM, Han WS, et al. BODIPY-functionalized gold nanoparticles as a selective fluoro-chromogenic chemosensor for imaging Cu^{2+} in living cells. Analyst 2010;135:2022–7.
[12] Virji S, Kojima R, Fowler JD, Villanueva JG, Kaner RB, Weiller BH. Polyaniline nanofiber composites with amines: novel materials for phosgene detection. Nano Res 2009;2:135–42.
[13] Leng B, Jiang JB, Tian H. A mesoporous silica supported Hg^{2+} chemodosimeter. AIChE J 2010;56:2957–64.
[14] Mu LX, Shi WS, Chang JC, Lee ST. Silicon nanowires-based fluorescence sensor for Cu (II). Nano Lett 2008;8:104–9.
[15] Chen QG, Zhou TY, He CY, Jiang YQ, Chen X. An in situ applicable colorimetric Cu^{2+} sensor using quantum dot quenching. Anal Methods 2011;3:1471–4.
[16] Wang HG, Sun L, Li YP, Fei XL, Sun MD, Zhang CQ, et al. Layer-by-layer assembled Fe_3O_4@C@CdTe core/shell microspheres as separable luminescent probe for sensitive sensing of Cu^{2+} ions. Langmuir 2011;27:11609–15.
[17] Lee MH, Lee SJ, Jung JH, Kim JS. Luminophore-immobilized mesoporous silica for selective Hg^{2+} sensing. Tetrahedron 2007;63:12087–92.
[18] Barja BC, Sara E, Bari M, Marchi C, Iglesias FL, Bernardi M. Luminescent Eu(III) hybrid sensors for in situ copper detection. Sensors Actuators B 2011;158: 214–22.
[19] Song YJ, Qu KG, Xu C, Ren JS, Qu XG. Visual and quantitative detection of copper ions using magnetic silica nanoparticles clicked on multiwalled carbon nanotubes. Chem Commun 2010;46:6572–4.
[20] Meng QT, Zhang XL, He C, He GJ, Zhou P, Duan CY. Multifunctional mesoporous silica material used for detection and adsorption of Cu^{2+} in aqueous solution and biological applications in vitro and in vivo. Adv Funct Mater 2010;20:1903–9.
[21] Kresge CT, Leonowicz ME, Roth WJ, Vartuli JC, Beck JS. Ordered mesoporous molecular sieves synthesized by a liquid-crystal template mechanism. Nature 1992;359:710–2.
[22] Rosenholm JM, Meinander A, Peuhu E, Niemi R, Eriksson JE, Sahlgren C, et al. Targeting of porous hybrid silica nanoparticles to cancer cells. ACS Nano 2009; 3:197–206.
[23] Song CX, Zhang XL, Jia CY, Zhou P, Quan X, Duan CY. A hybrid mesoporous material functionalized by 1,8-naphthalimide-base receptor and the application as chemosensor and absorbent for Hg^{2+} in water. Talanta 2010;81: 643–9.
[24] Zhou J, Wu W, Caruntu D, Yu MH, Martin A, Chen JF, et al. Synthesis of porous magnetic hollow silica nanospheres for nanomedicine application. J Phys Chem C 2007;111:17473–7.
[25] Barnham KJ, Masters CL, Bush AI. Neurodegenerative diseases and oxidative stress. Nat Rev Drug Discov 2004;3:205–14.
[26] Xu ZH, Zhang LK, Guo R, Xiang TC, Wu CZ, Zheng Z, et al. A highly sensitive and selective colorimetric and off–on fluorescent chemosensor for Cu^{2+} based on rhodamine B derivative. Sensors Actuators B 2011;156:546–52.
[27] Mu HL, Gong R, Ma Q, Sun YM, Fu EQ. A novel colorimetric and fluorescent chemosensor: synthesis and selective detection for Cu^{2+} and Hg^{2+}. Tetrahedron Lett 2007;30:5525–9.
[28] El-Safty SA, Ismail AA, Shahat A. Optical supermicrosensor responses for simple recognition and sensitive removal of Cu (II) Ion target. Talanta 2011; 83:1341–51.
[29] Torrado A, Walkup GK, Imperiali B. Exploiting polypeptide motifs for the design of selective Cu (II) ion chemosensors. J Am Chem Soc 1998;120: 609–10.
[30] Wang JG, Xiao Q, Zhou HJ, Sun PC, Ding DT, Chen TH. Anionic surfactant-templated mesoporous silica (AMS) nano-spheres with radially oriented mesopores. J Colloid Interf Sci 2008;323:332–7.
[31] Lakowicz JR. Quenching of fluorescence. Principles of fluorescence Spectroscopy. 3nd ed. New York: Springer; 2006. pp. 288–289.